ADVANCED MATERIALS INTERFACES
www.advmatinterfaces.de

In Situ Observations of Freestanding Single-Atom-Thick Gold Nanoribbons Suspended in Graphene

*Liang Zhao, Huy Q. Ta, Rafael G. Mendes, Alicja Bachmatiuk, and Mark H. Rummeli**

Bulk gold's attributes of relative chemical inertness, rarity, relatively low melting point and its beautiful sheen make it a prized material for humans. Recordings suggest it was the first metal employed by humans dating as far back to the late Paleolithic period ≈40 000 BC. However, at the nanoscale gold is expected to present new and exciting properties, not least in catalysis. Moreover, recent studies suggest a new family of single-atom-thick two-dimensional (2D) metals exist. This work shows single-atom-thick freestanding gold membranes and nanoribbons can form as suspended structures in graphene pores. Electron irradiation is shown to lead to changes to the graphene pores which lead to dynamic changes of the gold membranes which transition to a nanoribbon. The freestanding single-atom-thick 2D gold structures are relatively stable to electron irradiation for extended periods. The work should advance the development of 2D gold monolayers significantly.

1. Introduction

Noble-metal nanocrystals (NCs) have attracted significant attention as they exhibit fascinating properties and are therefore promising for applications in electronics, catalysis, photonics, sensing, and biomedicine.[1–6] As one of various kinds of noble-metal materials, gold (Au) shows exceptional stability with regard to chemical reactions. Recent experimental studies have shown that the physicochemical properties of Au NCs directly correlate with their size, dimensionality, crystal phase, shape, and surface properties.[7–13] For example, nanometer-sized Au particles display superior catalytic activity in the solvent-free aerobic oxidation of ethylbenzene and toluene as compared to inert bulk gold.[14,15] Theoretical and experimental studies indicate that two-dimensional (2D) gold could have exciting properties due to its anisotropic structure. Yang et al.[16] theoretically predicted a stable atomically thin gold monolayer with hexagonal symmetry. The bond energy was significantly augmented when going from a three-dimensional (3D) bulk form to a 2D monolayer, somewhat similar to the case of 3D diamond to 2D graphene. Antikainen et al. used density functional theory (DFT) to investigate the feasibility of 2D Au membranes in graphene pores.[17] The computation study showed Au atoms could move effortlessly from the top of graphene to its edge and over the surface of a 2D Au structure, to its open edge without a significant energy barrier. Thus, an atomically thin 2D gold layer would avoid getting trapped on the top of a 2D Au membrane owing to the lack of an energy barrier, and hence avoid growing additional layers.

It is difficult to obtain a 2D gold nanostructure through top-down exfoliation methods owing to gold's bulk structure having no intrinsic layers. In addition, large clusters of Au atoms would be more prone to trigger the growth of bulk Au (such as face-centered cubic (fcc), cubic close-packed (hcp), or body-centered cubic (bcc) phases) instead of a 2D film, due to the strong metallic bonds between gold atoms.[18–21] To facilitate the 2D anisotropic growth of gold, kinetic control over the growth a pathway by either slowing down the atom addition process or lowering the total free energy of the metal nanostructures is needed.[22–24] Experimentally, Fan et al. synthesized ultrathin Au square sheets with a unique hcp crystal phase over graphene oxide (GO). Au clusters on GO grew into Au square sheets by reducing $HAuCl_4$ with oleylamine (OAM). Electron beam irradiation was used to drive the transformation of the Au square sheet from an hcp to a fcc structure.[7,25] The thickness of these Au sheets was ≈5 nm. The fabrication of 2D Au from one to a few atomic layers in thickness remains challenging either supported or as a freestanding structure.

L. Zhao, Prof. A. Bachmatiuk, Prof. M. H. Rummeli
Key Laboratory of Advanced Carbon Materials and Wearable Energy Technologies of Jiangsu Province, College of Energy
Soochow Institute for Energy and Materials InnovationS
Soochow University
Suzhou 215006, China
E-mail: mhr1@suda.edu.cn

Dr. H. Q. Ta, Dr. R. G. Mendes, Prof. M. H. Rummeli
IFW Dresden
20 Helmholtz Strasse
Dresden 01069, Germany

Prof. A. Bachmatiuk, Prof. M. H. Rummeli
Centre of Polymer and Carbon Materials
Polish Academy of Sciences
M. Curie-Sklodowskiej 34, Zabrze 41-819, Poland

Prof. A. Bachmatiuk
Polish Center for Technology Development (PORT)
Ul. Stabłowicka 147, Wrocław 54-066, Poland

Prof. M. H. Rummeli
Institute of Environmental Technology
VŠB-Technical University of Ostrava
17. listopadu 15, Ostrava 708 33, Czech Republic

The ORCID identification number(s) for the author(s) of this article can be found under https://doi.org/10.1002/admi.202000436.

DOI: 10.1002/admi.202000436

Electron beam in STEM has been demonstrated as a powerful tool to create and engineer nanostructures with atomic precision. More recently, researchers have reported that monolayer metal membranes can be fabricated by selective e-beam ejection of specific elements from their compounds or alloys. Zhao et al. have created a monolayer Mo membrane by selectively ionizing Se atoms in a $MoSe_2$ monolayer.[26] It is worth noting that Wang et al. successfully fabricated freestanding monatomic thick Au membranes by electron beam dealloying of Au–Ag alloy inside transmission electron microscope (TEM) using a similar technique.[27]

Graphene, another material with significant promise,[28] has also been shown as a means to stabilize 2D atom-thick membranes. In this approach, pores in the graphene provide stabilizing edges to support freestanding exotic single-atom-thick 2D membranes. Zhao et al.[29] demonstrated freestanding single-atom-thick 2D Fe membranes supported in graphene pores. Electron irradiation (from the imaging beam) using an acceleration voltage of 80 kV was able to drive Fe atoms and clusters into pores in the monolayer graphene and form an ordered 2D structure with a square lattice. The technique has also been used to successfully form other single-atom-thick 2D structures, namely, freestanding graphene-like ZnO,[30] CuO,[31] and Cr.[32] The stabilization of 2D membranes in graphene occurs when the interaction between the (metal) atoms and the pore edge is exothermic and suitably directional.[33] Graphene fulfils this requirement as it prefers in-plane adsorption at its pore edges[17,34] rather than on-top adsorption.[35]

In this work, we expand the potential of the technique and demonstrate how opposing sides of a graphene pore can serve as support interfaces for single-atom-thick 2D gold nanoribbons. The 2D Au nanoribbons have a hexagonal lattice structure.

2. Results and Discussion

The sample was prepared by subliming $HAuCl_4$ over transferred graphene at elevated temperatures in high vacuum. In brief, graphene grown over a high-purity Cu substrate by chemical vapor deposition (CVD) was transferred to a standard lacey carbon Cu TEM grid, and then placed in a vial with small amount of $HAuCl_4$. The vial was evacuated to $\approx 10^{-6}$ mbar and then sealed by flame. The sealed vial then was subsequently heated at 350 °C for 12 h during which the $HAuCl_4$ sublimes and decomposes, leaving Au on the graphene surface.

Under close inspection in a TEM, pure Au can be found as small NCs on the surface of the graphene and as single atoms or small clusters at the edge of pores in graphene. Typical examples are provided in Figure S1 (Supporting Information). Energy-dispersive X-ray spectroscopy (EDS) was implemented to confirm the presence of Au (Figure S1g, Supporting Information). The samples showed an interesting Au crystal dynamic behavior at graphene edges and pores, in which an Au nanoparticle typically undergoes a variety of structural changes when exposed to the electron beam to yield an ordered 2D suspended freestanding crystalline ribbon. An example of the observed in situ dynamic changes and the formation of a single-atom-thick 2D Au nanoribbon is provided in **Figure 1**. Greater detail of the dynamic aspects can be seen in Movie 1 (Supporting Information).

The movie and Figure 1 show a high contrast Au NC with a trapezoidal shape suspended in a graphene pore. Three sides of Au NC are closely connected with edge of the graphene pore while the right side is exposed to the vacuum (Figure 1a). Under electron beam irradiation, the graphene material to the left of the Au NC is removed due to sputtering over a period of several minutes leaving the Au crystal bridging the top and bottom parts of the remaining section of the graphene pore, viz, it is a suspended nanoribbon. This process is seen in Figure 1a–c. With further irradiation the contaminant carbon materials that reside near the top Au crystal–graphene interface are also sputtered away such that by 316 s a clean Au–graphene interface exists. During this process the ribbon length increases and to compensate for the increased bridging distance, the Au ribbons narrow down to a width of four atoms thus providing extra atoms to increase the ribbon length and maintain an interface to the graphene (Figure 1c–e). With further irradiation,

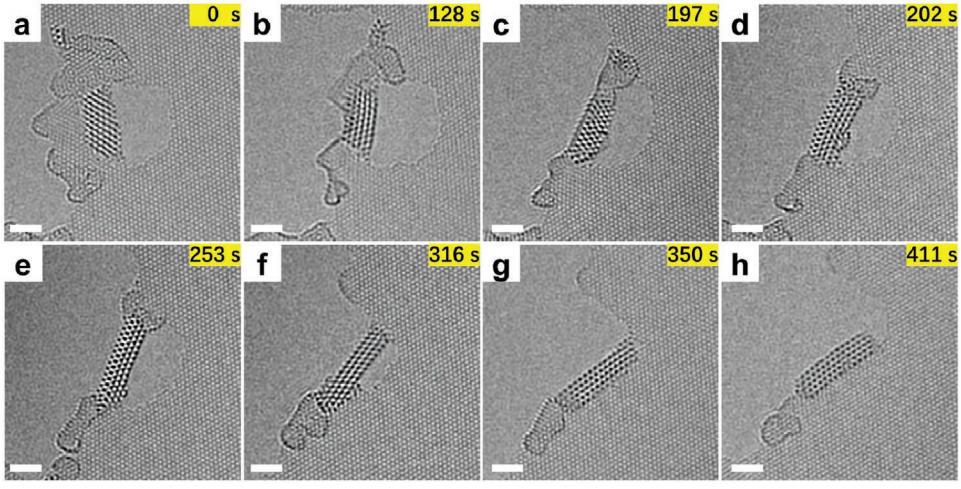

Figure 1. A series of transmission electron microscope (TEM) images showing the formation of suspended two-dimensional (2D) single-atom-thick Au nanoribbon at the edge of graphene. All scale bars = 1 nm.

the upper section of the remaining pore continues to etch and in this case the Au ceases to elongate, instead the top Au–graphene bridge interface moves to the right where the remaining pore width is less. This process continues until long side of the Au nanoribbon then interfaces with the graphene (Figure 1f–h). All these processes occur over a timespan just over 400 s. We postulate the changes occur to minimize energy and, thus maximize stability. The three key stages are loss of graphitic material at left side of the graphene pore, a shift to form a single-atom-thick 2D Au ribbon forming a freestanding bridge which later swings over to the right to fully interface on to the other side of the graphene pore as shown in **Figure 2**a–c. Diffraction data from the Fourier domain show a set of threefold hexagonal reflex spots (e.g. Figure 1d–f) for the Au nanoribbon concomitant with the observed hexagonal close packed atomic structure of the Au nanoribbon. Evaluation of the d-spacing from the reflex sets indicates some anisotropy with the anisotropy along long axis of the Au nanoribbon being greatest. The anisotropy is confirmed by studies on the atomic spacing of the Au ribbon at various dynamic stages in the pore collected directly from micrographs. The data can be seen in Figure S2 (Supporting Information) and confirm a larger atomic spacing along the long axis of the Au ribbon and is attributed to strain occurring along the bridging axis of the Au ribbon to the graphene pore.

From the d-spacing data, with correction made using published values for graphene lattice data, we obtain an average lattice constant of 2.71 ± 0.01 Å for the Au nanoribbon (see Figure S6 and Table S1, Supporting Information). We discuss the lattice spacing a little later in greater detail. We now turn to investigations on the Au nanoribbons thickness. To do this, we prepare image simulations and then compare the relative intensity profiles across graphene and over the Au nanoribbons from the simulations with experimental micrographs. The intensities are normalized to the graphene intensity profiles.

Figure 3 shows the intensity profile for the experimental case (Figure 3a) and an image simulation for a single-atom-thick 2D Au nanoribbon (Figure 3b). Figure 3c,e show the stick and ball structures for easy viewing. Figure 3d shows the relative intensity profiles for the experimental data and image simulation. The intensity profiles match each other very well. This can be compared with the simulations for Au nanoribbons with two and three atom-thick structures as shown in **Figure 4**, where

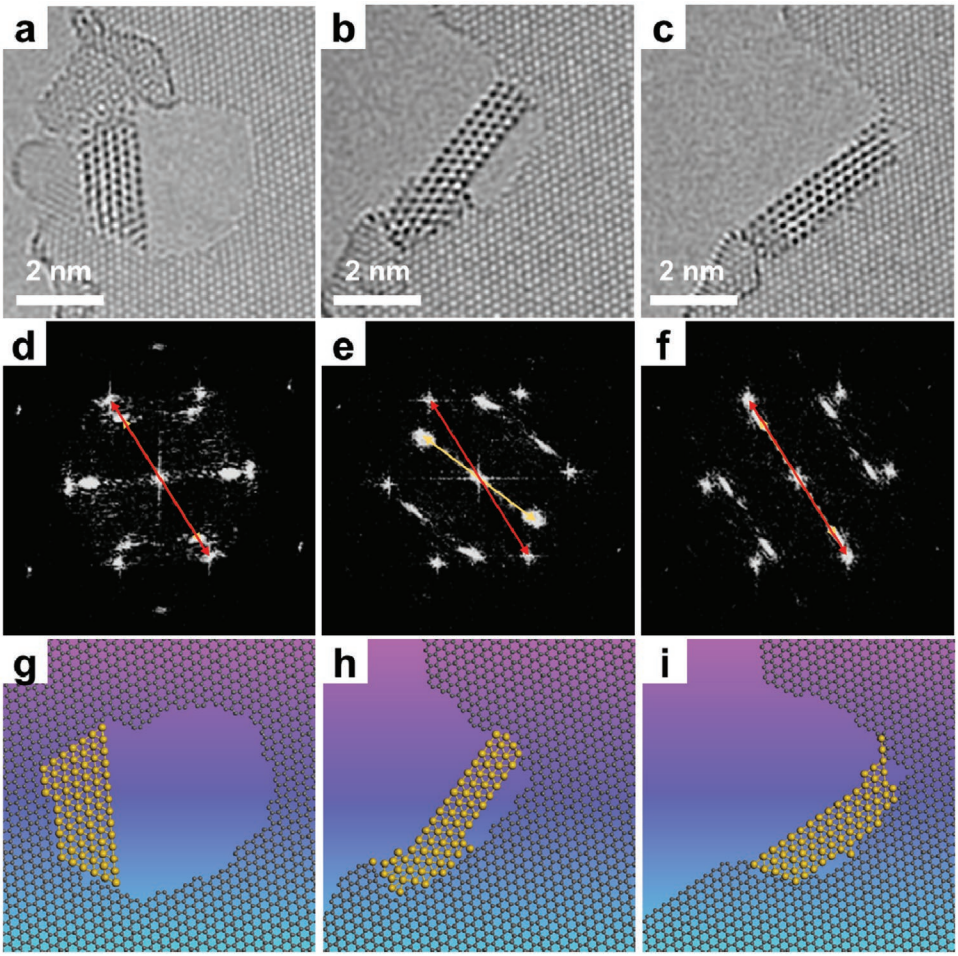

Figure 2. Three key stages of the dynamic process. High-resolution transmission electron microscope (HRTEM) images show a) single-atom-thick Au crystal suspended in a graphene hole; b) suspended two-dimensional (2D) single-atom-thick Au nanoribbon; c) Au nanoribbon attaching to the graphene edge; d–f) the fast Fourier transform of the structures corresponding to (a–c) show lattice relationship between graphene (red arrow) and Au nanostructures (yellow arrow); g–i) the stick and ball model (a–c), respectively.

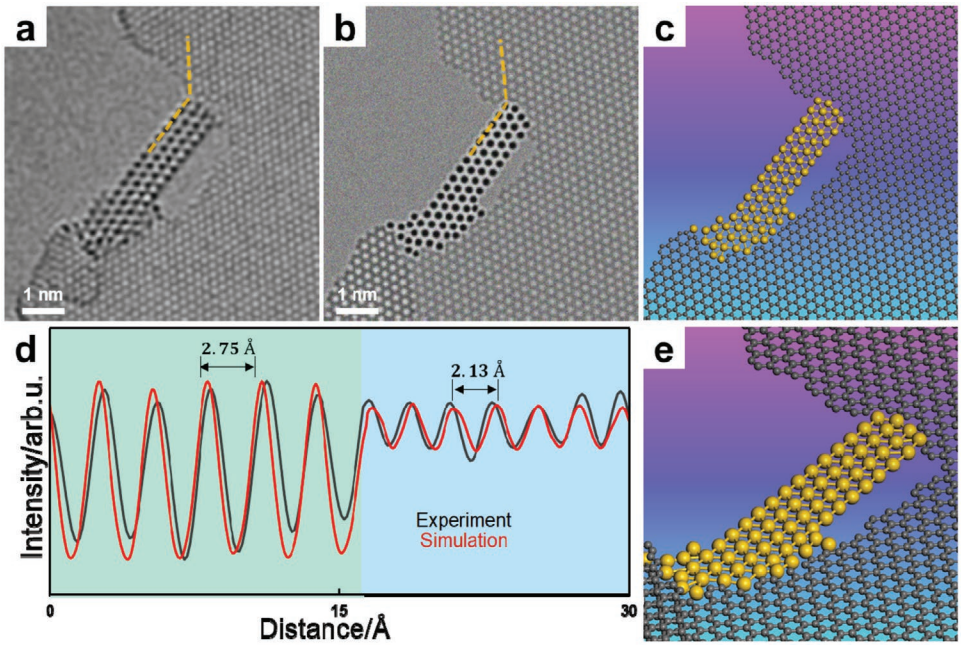

Figure 3. a) High-resolution transmission electron microscope (HRTEM) image showing a single-atom-thick Au nanoribbon suspended between two graphene edges. b) Image simulation of a monoatomic thick Au nanoribbon. c,e) Top view and side view of the stick and ball model of the suspended Au nanoribbon. d) Normalized intensity profiles from the image simulation (red line) and experimental image (black line), corresponding to marked profiles in orange-dashed lines in (a,b). The intensity profiles match, confirming that the Au nanoribbon is a single-atom-thick Au nanoribbon.

the profile intensities for two- and three-atom-thick structures are a poor fit to the experimental data. This indicates the Au nanoribbons comprise 2D single-atom-thick freestanding nanoribbons. Moreover, the fit between simulation and experiment confirms the ribbons are from Au. To highlight this, Figure S3 (Supporting Information) shows image simulations and relative intensity profiles for the single-atom-thick Au ribbon with similar ribbons from Si, Cu, and Fe (the possible contaminants in the system). Only the Au simulation matches the experimental data as expected.

We also examine the ribbon at the later stage when its right-hand long side interfaces with the graphene pore (Figure 1g). Relative intensity profiles between image simulations and experiment confirm the structure remains one Au atom-thick as shown in **Figure 5**.

The formation of the single-atom-thick freestanding 2D Au nanoribbon was not an isolated event. We found numerous ribbons during the course of this study. Two further examples are provided in Figure S4 (Supporting Information). We did not observe any nanoribbons with a width below four atoms wide. All nanoribbons showed a hexagonal close-packed structure. Moreover, relative intensity measurements with image simulations confirmed all the 2D Au nanoribbons to be one-atom-thick and freestanding (e.g. Figure S5, Supporting Information).

We also examined the stability of the freestanding 2D single-atom-thick Au nanoribbon against the electron irradiation. Despite extended irradiation periods the Au nanoribbon structures remained remarkably stable and dynamic changes (e.g. Figure 1) seem to be driven more by changes to the graphene (e.g. sputtering). This is different from other studies with freestanding 2D single-atom-thick metal and metal oxide membranes. Zhao et al. observed this collapse of a 2D free-standing atom-thick Fe membrane under prolonged electron beam irradiation.[29] Quang et al. also showed a freestanding single-atom-thick 2D graphene-like ZnO membrane to collapse extended irradiation.[30] The stability of the 2D single-atom-thick Au nanoribbons is in keeping with a molecular dynamics study examining single-atom-thick 2D gold structures, which show such 2D Au membranes are stable up to temperatures of up to 1400 K.[16] Another theoretical work by Antikainen et al. suggests that the collapse of such 2D membranes to 3D nanoparticles requires elevated temperatures.[17] Another theoretical work by Yang et al., apart from pointing to stable single-atom-thick 2D Au membranes, predicts a structure corresponding to the bulk Au (111) face-centered cubic lattice as this close-packed lattice maximizes the aerophilic interactions.[16] In this study, we observe the predicted close-packed lattice, viz., a single layer of the Au (111) lattice. Moreover, the same theoretically suggested optimized lattice constants of 2.755 Å which is a little larger than our average measured lattice spacing of 2.71 ± 0.01 Å.

A recent theoretical work by Nevalaita et al. indicated a stable 2D metal patch could be achieved by interfacing to graphene edges.[33] Consequently, we examined the interface between the 2D single-atom-thick Au nanoribbon and the graphene edge. Careful examination shows several Au atom configurations at armchair or zigzag edges can be seen in Figure S7 (Supporting Information). Statistics for the four observed configurations for Au atoms linked to the hollow (C1) and bridge (C2) sites of armchair graphene, and hollow (C3) and top (C4) sites of zigzag graphene with the corresponding stick and ball model are given in **Figure 6**. The most frequent bonding configurations occur for C4 and C3, respectively, which have the largest bonding energy (3.4 and 3.3 eV, respectively).[36]

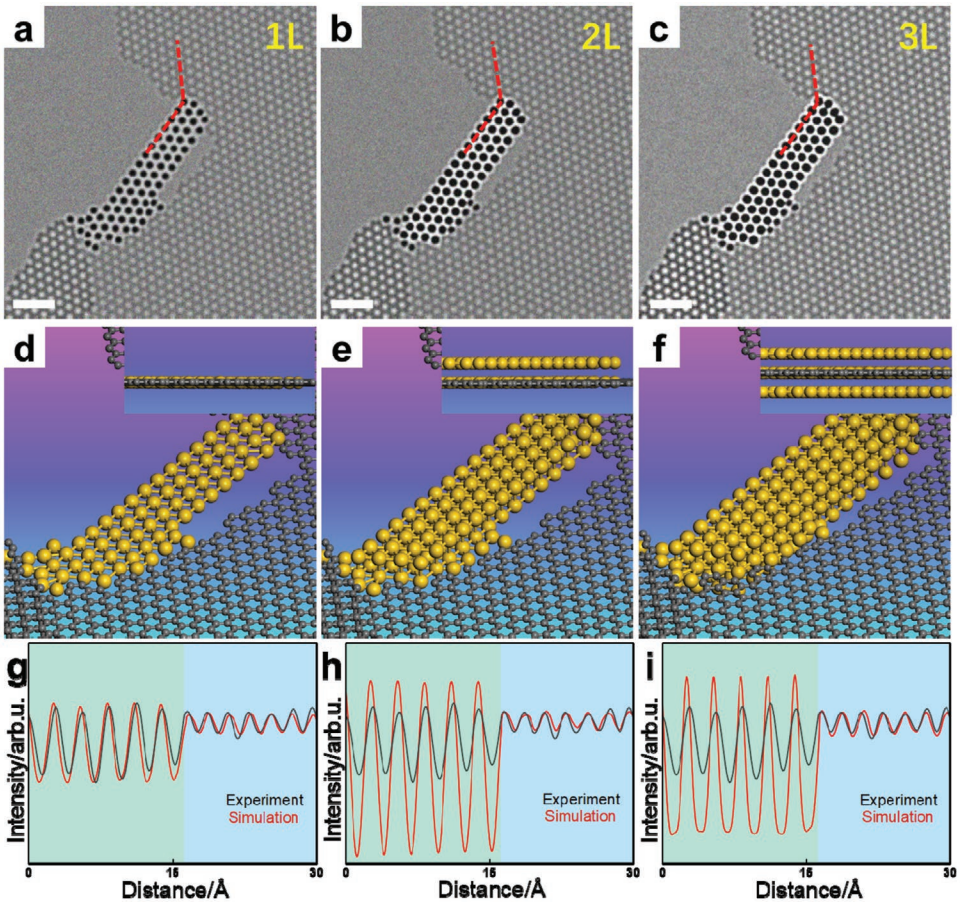

Figure 4. Comparisons of image simulations with different Au nanoribbon atomic layer thickness. a) Monolayer; b) bilayer; c) trilayer; d–f) stick and ball models, insets: side view of the stick and ball models. g–i) The relative intensity profile from the image simulation (red line) and experimental image (black line), corresponding to the orange dash lines in panels (a–c), respectively. All scale bars = 1 nm.

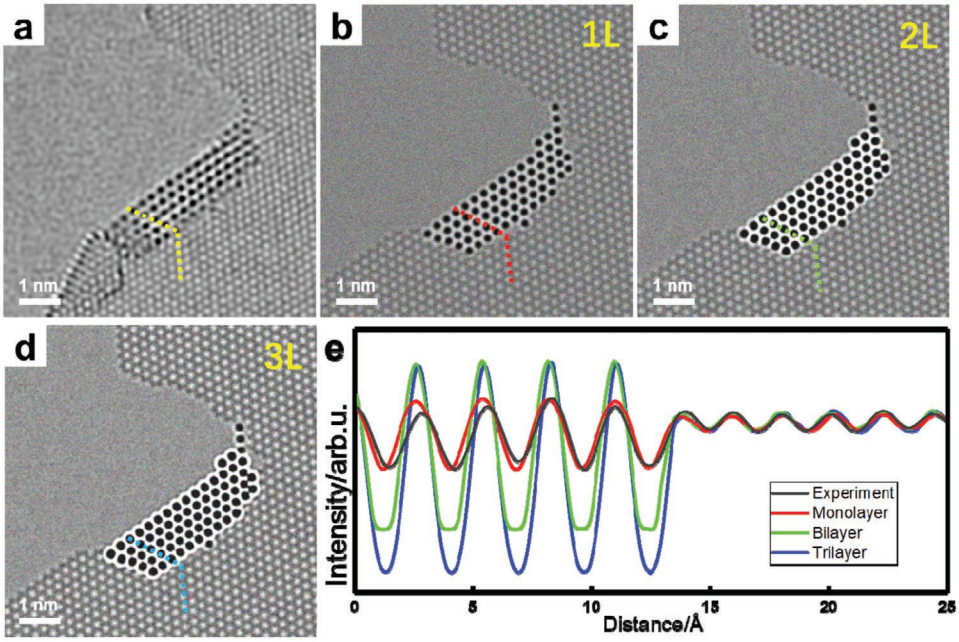

Figure 5. a) High-resolution transmission electron microscope (HRTEM) image showing an Au nanoribbon anchored to the edge of graphene. Comparisons of image simulations with different Au nanoribbon layers; b) monolayer; c) bilayer; d) trilayer, respectively; e) normalized intensity profiles from the image simulation and experimental image, corresponding to marked profiles in dashed lines in panels (a–d). The experimental data (black curve) have the best fit for monolayer simulation (red curve) confirming 2D one atom-thick Au.

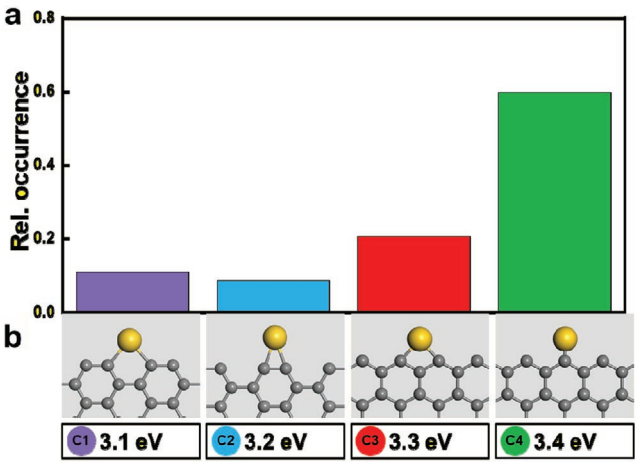

Figure 6. Comparison of four different configurations, C1, C2, C3, and C4 of an Au atom located at a graphene armchair edge (C1 and C2) and zigzag edge (C3 and C4). a) The relative occurrence of each configuration. (b) Stick-ball models and corresponding binding energies from reference[36].

3. Conclusion

In summary, we provide experimental evidence for the formation of freestanding single-atom-thick 2D Au nanoribbons suspended at graphene edges. Their structures, that of the top monolayer of bulk Au (111) and their lattice spacing, match very well with previous theoretical predictions.[17] The width of the 2D Au nanoribbons vary from seven to four atoms in width. The 2D Au nanoribbons exhibit significant stability under electron irradiation (at 80 kV). Theoretical predictions suggest 2D single-atom-thick Au structures are metallic and diamagnetic with metallic bonds holding the gold atoms together in the 2D plane.[17] Interesting electrical, mechanical, and thermal properties are predicted for 2D gold layers and this work should advance the development of 2D Au monolayers significantly.

4. Experimental Section

Sample Preparation: The graphene was obtained by thermal CVD over high purity copper (99.99%) and is described elsewhere.[35] After synthesis, the graphene was transferred to standard lacey carbon Cu TEM grids. The TEM grid with graphene was then placed in a glass vial along with a nominal amount of $HAuCl_4$. The vial was evacuated to $\approx 10^{-6}$ mbar and sealed. The sealed vial was heated to 350 °C for 12 h. This process, based on the technique developed in ref. [30], sublimes and decomposes the $HAuCl_4$ to leave copious Au atoms on the graphene surface. Prior to placing the sample in the TEM for the in situ experiments, the specimen was annealed under vacuum ($<10^{-6}$ mbar) overnight at 160 °C. The $HAuCl_4$ was purchased from Alfa Aesar and has a purity of 99.9%.

In Situ TEM Experiments: The high-resolution TEM (HRTEM) images of Au nanoribbons were obtained on a FEI Titan Cubed Themis G2 30–300 TEM equipped with spherical (Cs) aberration correction for the objective lens and monochromator and was operated at 80 kV. The current density was typically 3.8 nA nm^{-2}. All studies were conducted at room temperature with a pressure of $\approx 10^{-7}$ mbar.

Image Simulation: The HRTEM image simulations were performed using JEMS software. For the simulations, an accelerating voltage of 80 kV and an energy spread of 0.2 eV were used. The chromatic aberration Cc was set to 1 mm, and the spherical aberration Cs was set to 1 µm. A defocus between 4 and 5 nm was used, and a defocus spread of 3 nm was implemented. These values are consistent with the experimental conditions used.

Supporting Information

Supporting Information is available from the Wiley Online Library or from the author.

Acknowledgements

This work was financially supported by the National Science Foundation China (NSFC, Project 51802207 and Project 51672181), the National Science Center, Poland, within the framework of the Opus program (Grant Agreement No. 2015/19/B/ST5/03399), and the Czech Republic under the ERDF program "Institute of Environmental Technology-Excellent Research" (No.CZ.02.1.01/0.0/0.0/16_019/0000853). M.H.R. thanks the Sino-German Research Institute for support (Project No. GZ 1400).

Conflict of Interest

The authors declare no conflict of interest.

Keywords

electron beam irradiation, gold nanoribbons, in situ TEM, single-atom-thick

Received: March 10, 2020
Revised: April 17, 2020
Published online:

[1] C. Louis, O. Pluchery, *Gold Nanoparticles for Physics, Chemistry and Biology*, World Scientific, Singapore **2017**.
[2] X. Huang, I. H. El-Sayed, W. Qian, M. A. El-Sayed, *J. Am. Chem. Soc.* **2006**, *128*, 2115.
[3] C. Wang, Y. Hu, C. M. Lieber, S. Sun, *J. Am. Chem. Soc.* **2008**, *130*, 8902.
[4] N. Li, P. Zhao, D. Astruc, *Angew. Chem., Int. Ed.* **2014**, *53*, 1756.
[5] N. L. Rosi, D. A. Giljohann, C. S. Thaxton, A. K. R. Lytton-Jean, M. S. Han, C. A. Mirkin, *Science* **2006**, *312*, 1027.
[6] Y. Huang, M. Zhao, S. Han, Z. Lai, J. Yang, C. Tan, Q. Ma, Q. Lu, J. Chen, X. Zhang, Z. Zhang, B. Li, B. Chen, Y. Zong, H. Zhang, *Adv. Mater.* **2017**, *29*, 1700102.
[7] Z. Fan, Y. Zhu, X. Huang, Y. Han, Q. Wang, Q. Liu, Y. Huang, C. L. Gan, H. Zhang, *Angew. Chem., Int. Ed.* **2015**, *54*, 5672.
[8] N. Tian, Z. Y. Zhou, S. G. Sun, Y. Ding, L. W. Zhong, *Science* **2007**, *316*, 732.
[9] Y. Chen, Z. Fan, Z. Luo, X. Liu, Z. Lai, B. Li, Y. Zong, L. Gu, H. Zhang, *Adv. Mater.* **2017**, *29*, 1701331.
[10] Y. Xia, Y. Xiong, B. Lim, S. E. Skrabalak, *Angew. Chem., Int. Ed.* **2009**, *48*, 60.
[11] H. Yuan, W. Ma, C. Chen, J. Zhao, J. Liu, H. Zhu, X. Gao, *Chem. Mater.* **2007**, *19*, 1592.
[12] S. Link, M. A. El-Sayed, *Int. Rev. Phys. Chem.* **2000**, *19*, 409.

[13] C. J. Murphy, T. K. Sau, A. M. Gole, C. J. Orendorff, J. Gao, L. Gou, S. E. Hunyadi, T. Li, *J. Phys. Chem. B* **2005**, *109*, 13857.
[14] Y. Liu, C. N. Jia, J. Yamasaki, O. Terasaki, F. Schüth, *Angew. Chem., Int. Ed.* **2010**, *49*, 5771.
[15] Y. He, J. C. Liu, L. Luo, Y. G. Wang, J. Zhu, Y. Du, J. Li, S. X. Mao, C. Wang, *Proc. Natl. Acad. Sci. USA* **2018**, *115*, 7700.
[16] L. M. Yang, M. Dornfeld, T. Frauenheim, E. Ganz, *Phys. Chem. Chem. Phys.* **2015**, *17*, 26036.
[17] S. Antikainen, P. Koskinen, *Comput. Mater. Sci.* **2017**, *131*, 120.
[18] X. Huang, S. Tang, X. Mu, Y. Dai, G. Chen, Z. Zhou, F. Ruan, Z. Yang, N. Zheng, *Nat. Nanotechnol.* **2011**, *6*, 28.
[19] P. Söderlind, O. Eriksson, B. Johansson, J. M. Wills, A. M. Boring, *Nature* **1995**, *374*, 524.
[20] Z. Fan, H. Zhang, *Chem. Soc. Rev.* **2016**, *45*, 63.
[21] P. Koskinen, T. Korhonen, *Nanoscale* **2015**, *7*, 10140.
[22] X. Sun, S. Dong, E. Wang, *Angew. Chem., Int. Ed.* **2004**, *43*, 6360.
[23] S. Porel, S. Singh, T. P. Radhakrishnan, *Chem. Commun.* **2005**, *18*, 2387.
[24] C. Lofton, W. Sigmund, *Adv. Funct. Mater.* **2005**, *15*, 1197.
[25] X. Huang, H. Li, S. Li, S. Wu, F. Boey, J. Ma, H. Zhang, *Angew. Chem., Int. Ed.* **2011**, *50*, 12245.
[26] X. Zhao, J. Dan, J. Chen, Z. Ding, W. Zhou, K. P. Loh, S. J. Pennycook, *Adv. Mater.* **2018**, *30*, 1707281.
[27] X. Wang, C. Wang, C. Chen, H. Duan, K. Du, *Nano Lett.* **2019**, *19*, 4560.
[28] C. Tan, X. Cao, X. J. Wu, Q. He, J. Yang, X. Zhang, J. Chen, W. Zhao, S. Han, G. H. Nam, M. Sindoro, H. Zhang, *Chem. Rev.* **2017**, *117*, 6225.
[29] J. Zhao, Q. Deng, A. Bachmatiuk, G. Sandeep, A. Popov, J. Eckert, M. H. Rummeli, *Science* **2014**, *343*, 1228.
[30] H. T. Quang, A. Bachmatiuk, A. Dianat, F. Ortmann, J. Zhao, J. H. Warner, J. Eckert, G. Cunniberti, M. H. Rümmeli, *ACS Nano* **2015**, *9*, 11408.
[31] K. Yin, Y. Y. Zhang, Y. Zhou, L. Sun, M. F. Chisholm, S. T. Pantelides, W. Zhou, *2D Mater* **2017**, *4*, 1.
[32] H. T. Quang, X. Yang, S. Liu, R. G. Mendes, T. Gemming, Y. Liu, L. Liu, J. H. Choi, Z. Liu, A. Bachmatiuk, M. H. Rummeli, *Nano Lett.* **2020**, https://doi.org/10.1021/acs.nanolett.0c01082.
[33] J. Nevalaita, P. Koskinen, *Nanoscale* **2019**, *11*, 22019.
[34] S. Malola, H. Häkkinen, P. Koskinen, *Appl. Phys. Lett.* **2009**, *94*, 043106.
[35] L. Pastewka, S. Malola, M. Moseler, P. Koskinen, *J. Power Sources* **2013**, *239*, 321.
[36] H. Wang, K. Li, Y. Cheng, Q. Wang, Y. Yao, U. Schwingenschlögl, X. Zhang, W. Yang, *Nanoscale* **2012**, *4*, 2920.